Molecular Self-Assembly on Surfaces of Organic Conducting Salts: Epitaxial Monolayer Films of Naphthalene on the (001) Surface of $(TMTSF)_2PF_6$

P. N. Bartlett,[†,*] J. W. Essex,[†] H.-J. Koo,[‡] I. S. Nandhakumar,[†] N. Robertson,[§] and M.-H. Whangbo[‡]

Department of Chemistry, University of Southampton, Southampton SO17 1BJ, U.K., Department of Chemistry, University of Edinburgh, Edinburgh EH9 3JJ, U.K., and Department of Chemistry, North Carolina State University, Raleigh, North Carolina 27695-8204

Received: January 4, 2000; In Final Form: March 17, 2000

Pristine and naphthalene-adsorbed (001) surfaces of the organic conducting salt $(TMTSF)_2PF_6$ were examined by scanning tunneling microscopy (STM) to determine the structure of epitaxial monolayer films of naphthalene on the (001) surface. The observed STM images were interpreted by calculating partial electron density plots of the surface, and for naphthalene-adsorbed surfaces, by carrying out Monte Carlo simulations for the adsorption of a naphthalene molecule on the surface. The STM images recorded for the pristine (001) surface correspond to the cation layer of $(TMTSF)_2PF_6$, and each circular bright spot of the molecular-resolution STM images represents the three hydrogen atoms of the most protruding methyl group of a TMTSF molecule on the (001) surface. Naphthalene molecules adsorbed on this surface form a pseudomorphic (1×1) overlayer structure with respect to the underlying substrate. The naphthalene overlayer shows mechanical stability against etching by the scanning tip. An identical overlayer structure of naphthalene was obtained from several different preparation methods. On the cation-layer (001) surface naphthalene is adsorbed on each "four-methyl-step" defined by four methyl groups of two adjacent TMTSF molecules within each TMTSF stack.

1. Introduction

The modification of surfaces with organic monolayers and thin films is of fundamental and technological importance and has broad implications to electrocatalysis,[1] biological and chemical sensors,[2] molecular recognition,[3] supramolecular chemistry,[3] and the field of molecular electronics.[4] Thin films of organic materials have predominantly been used as corrosion inhibitors and metal plating bath additives.[5,6] Current interests in these materials stem from their potential for systematically tailoring electronic and optical properties of surfaces by changing the size, shape, or functional groups of organic molecules.[7] Such modifications may lead to useful materials for technological applications in the arena of molecular electronic devices.[7] In this context, considerable attention has been paid to studying the structure, stability, nucleation/growth, and structure−property correlations of organic thin films on solid surfaces under both ultrahigh vacuum[8] conditions and in electrolyte solutions.[9−11] Highly ordered two-dimensional (2D) organic monolayer and ultrathin films are commonly prepared on well-defined flat substrates by employing solution-based methods[12] or by using vacuum deposition techniques such as organic molecular beam epitaxy.[13] Recently, the electronic and molecular surface structures of organic conducting salts have been the subject of extensive ex-situ examinations by scanning tunneling microscopy (STM) and atomic force microscopy (AFM) in air.[14−17] Carter et al.[18] and Bartlett et al.[19] have shown that these techniques can be employed to study surface transformations of these materials in solution as a function of the applied electrode potential. To the best of our knowledge, however, organic conducting salts have not been used as substrate surfaces in the study of molecular adsorption processes.

The adsorption of naphthalene has been intensively investigated on surfaces of graphite[20,21] and transition metals by STM in solution[22−24] and by various ultrahigh vacuum techniques.[25,26] Thus, naphthalene was chosen for overlayer formation in the present study. The organic conducting salts $(TMTSF)_2X$, where X is a monovalent anion such as PF_6^- or ClO_4^- and TMTSF is tetramethyltetraselenafulvalene, have been extensively studied.[27] These salts can be obtained in a single crystalline phase as high-quality single crystals with flat and crystallographically well-defined surfaces, so they are excellent model compounds for adsorption studies by scanning probe techniques. In the present work we report the first results of a detailed and systematic STM examination, performed in-situ as well as ex-situ, on well-ordered monolayer films of naphthalene grown on the (001) surface of $(TMTSF)_2PF_6$. To interpret the observed STM images, we performed partial electron density plot calculations[28−31] for the pristine and naphthalene-adsorbed (001) surfaces of $(TMTSF)_2PF_6$ using the extended Hückel tight-binding (EHTB) method,[32] and carried out Monte Carlo simulations for the adsorption of a naphthalene molecule on the (001) surface of $(TMTSF)_2PF_6$.

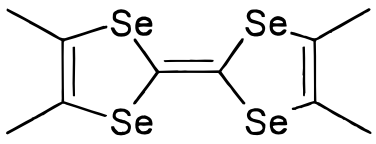

TMTSF

[†] University of Southampton.
[‡] North Carolina State University.
[§] University of Edinburgh.
* To whom correspondence should be addressed.

10.1021/jp000013z CCC: $19.00
Published on Web 07/19/2000

2. Experimental Section

Materials. High-quality single crystals of $(TMTSF)_2PF_6$ with optically flat surfaces were grown by standard electrochemical oxidation of TMTSF (Aldrich, 10 mg in 5 mL tetrachloroethane (TCE) in an H-shaped Pyrex glass cell in a solution of 1,1,2-TCE 0.1 M tetrabutylammonium (TBA)-PF_6 (Aldrich, 0.5 g in 10 mL TCE) at a platinum wire electrode (0.25 mm × 10 mm) at an applied constant current of 1 μA over a period of 3−5 days. This constant current technique produced long, shiny-black, needle-shaped crystals with typical dimensions of 5 × 1 × 0.3 mm. It has been demonstrated that the largest crystal face corresponds to the (001) surface with the needle axis parallel to the [100] crystallographic direction.[18]

Apparatus. The STM measurements were performed using a commercial Pico-STM system (Molecular Imaging Co.) interfaced with an EC-100 series controller (Molecular Imaging Co.) under ambient conditions in air and under potential control in solution. Mechanically cut Pt/Ir tips from a 0.25 mm diameter Pt (80%)/Ir (20%) wire were employed for ex-situ STM measurements, whereas electrochemically etched Pt/Ir tips (in 2 M $CaCl_2$ solutions at 35 V AC) coated with Apiezon wax were used for in-situ STM investigations. It has been shown that STM images obtained from soft surfaces such as organic conducting salts and layered transition-metal chalcogenides can be dominated by tip-induced surface deformations leading to differences in the fine structure of the images.[29] To exclude this possibility, we have therefore imaged pristine surfaces of $(TMTSF)_2PF_6$ by STM under varying tunneling conditions. Images were obtained in both constant-current as well as constant-height mode with bias voltages ranging between +400 and −400 mV and tunneling set-point currents varying between 0.5 and 5 nA. No significant differences were observed between the images obtained under the different imaging conditions, and high-quality STM images of the clean $(TMTSF)_2PF_6$ surface as well as of the naphthalene-covered surface were produced at bias voltages of either polarity. The tip was maintained at virtual ground and the bias voltage applied to the sample. The conditions reported in the figure legends were those which were found to give the best experimental resolution. All of the images presented are unfiltered and unprocessed unless otherwise stated in the figure caption. The calibration of the piezoelectric scanner in the *xy* plane was carried out using two different standards: highly oriented pyrolytic graphite and the $(\sqrt{3} \times \sqrt{3})R30°$ of bisulfate/sulfate on Au(111). The *z* calibration of the piezoelectric scanner was performed by imaging the Au atomic step height (0.235 nm). Because of thermal drift and inclination of the sample with respect to the tip and nonlinear effects of the piezodrive, the accuracy of STM data is in the limit of ±5%. To minimize the influence of thermal drift on image parameters, images were collected in the left-to-right and right-to-left scan directions and the averaged values were used for image characterization. To exclude the possibility of multiple tip effects and imaging artifacts, the scan direction was varied between successive image scans and a comparison was made between various images.

Before each STM experiment, a crystal of $(TMTSF)_2PF_6$ was mounted on a metal support with quick-drying conducting silver paint (Agar Scientific) and the STM tip was placed with the aid of an optical microscope at a flat and shiny area on the crystal surface. To remove dust particles from the surface, the crystal was rinsed with deionized water and subsequently dried in a stream of nitrogen prior to each experiment. Otherwise, no other form of surface pretreatment was applied. In-situ STM measurements were performed in a Kel-F STM cell which has been specifically adapted for this type of substrate and has been described in detail elsewhere.[19] It was ensured that only the *ab* (001) face of $(TMTSF)_2PF_6$ was in contact with the electrolyte solution while the crystal edges as well as the metal support disk were insulated with a silicon compound (Dow Corning, R4−3117 conformal coating). The electrolyte solution was not deaerated with nitrogen prior to the experiment because the electrochemical cell was open to air. A silver wire was used as a quasi-reference electrode and all electrode potentials are reported against it. A platinum wire directly immersed in the cell served as a counter electrode.

Preparation of Naphthalene Overlayers. Ordered naphthalene overlayers were grown by either spontaneous 2D condensation in solution under potential control and at open circuit potential or by vacuum sublimation. During deposition studies performed in-situ, the crystal was maintained near its rest potential of −400 mV versus Ag/Ag^+. The electrolyte solutions were prepared from propylene carbonate (B&J Brand, Fluka) and TBA-PF_6 (0.1 M), saturated with naphthalene. Nucleation and growth studies performed at open-circuit potential values were carried out in saturated solutions of naphthalene in phenyloctane (Aldrich), which is a nonpolar solvent. Sublimation from the vapor phase was carried out in a Schlenk tube at pressures of 2×10^{-2} Torr with the $(TMTSF)_2PF_6$ substrate being suspended from a Pt wire approximately 4−5 cm above a few naphthalene crystals which were heated with a hot air gun. Deposition times varied between 2 and 3 min. Each deposition method produced identical naphthalene overlayer structures.

Potentiometric Measurements. We also performed potentiometric measurements on working electrodes constructed from single crystals of $(TMTSF)_2PF_6$. To make electrical contact the crystal was attached to platinum wire sealed in a glass capillary with conducting silver-loaded paint. The contact and the crystal edges were then insulated with enamel paint (Humbrol), leaving only the largest (001) crystal face exposed. The electrodes were visually inspected under an optical microscope and their resistance was measured with a digital voltmeter prior to insulation. Variations in cell potential as a function of the anion concentration were measured with a high-input impedance differential amplifier circuit with a nominal leakage current of 0.15 pA. Solutions of TBA-PF_6 in propylene carbonate in the concentration range of $10^{-3}-10^{-1}$ M were used to determine the electrode response toward the reference ion PF_6^-. A silver wire was employed as a quasi-reference electrode and a platinum gauze electrode served as a counter electrode. The potential of the silver wire was calibrated against a saturated calomel electrode to ensure its potential stability under the given experimental conditions.

Calculations and Simulations. Determination of the potential adsorption sites for naphthalene was accomplished by performing Monte Carlo simulations of a single naphthalene molecule adsorbed onto a $(TMTSF)_2PF_6$ surface. A Silicon Graphics Indy workstation was employed together with a BOSS (W. L. Jorgensen, BOSS Version 3.8, Yale University, 1997) modeling program. A small section of the cation-terminated $(TMTSF)_2PF_6$ surface was constructed, and treated as rigid throughout the simulations. The intermolecular interactions between the surface and the naphthalene molecule were modeled using Lennard−Jones potential functions, the parameters being assigned by reference to similar atom types in the optimized potentials for liquid simulations (OPLS) force field provided with the BOSS program. Coulombic interactions were not included in the calculations because of the difficulty in deriving partial atomic

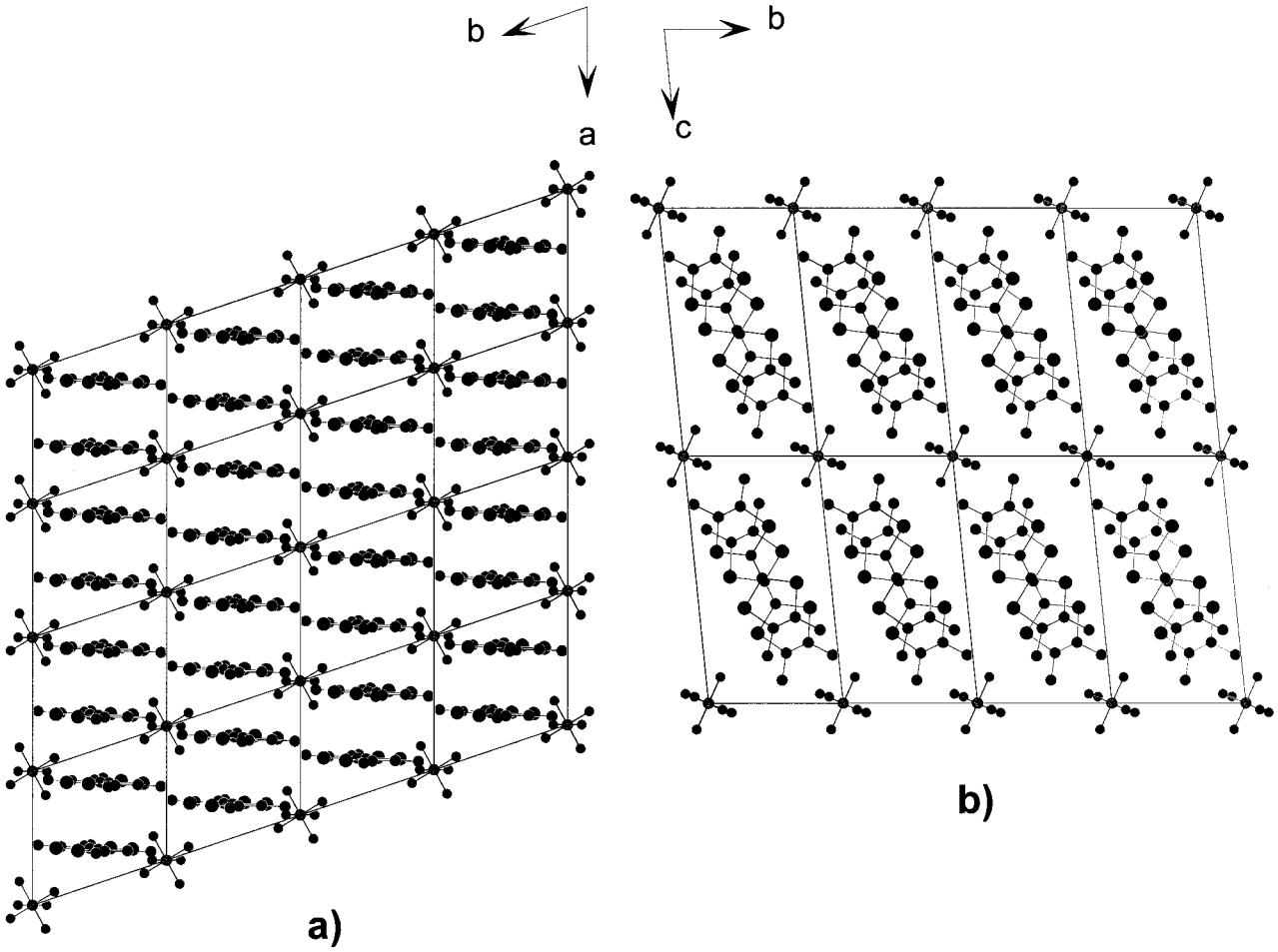

Figure 1. Schematic projection views of the crystal structure of $(TMTSF)_2PF_6$ on (a) the (001) plane (i.e., *ab* plane) and (b) the (100) plane (i.e., *bc* plane).

charges for the TMTSF molecules, which formally have a charge of +0.5. A Monte Carlo simulated annealing protocol was used to determine the preferential adsorption sites in which 10 000 Monte Carlo trial moves of a single naphthalene molecule were performed at 300, 200, 100, and finally 1 K. In an attempt to sample the energy surface reliably, this procedure was repeated 5 times, with each annealing run starting from the final configuration of the preceding calculation.

To interpret the STM images recorded for the pristine (001) surface of $(TMTSF)_2PF_6$, we calculated the partial electron density plots[28−31] $\rho(r_0, E_f)$ for an isolated cation layer by using the CAESAR program package.[33] To interpret the STM images recorded for the naphthalene-adsorbed (001) surface of $(TMTSF)_2PF_6$, we calculated the partial electron density plots for model bilayers which mimic a monolayer of naphthalene molecules adsorbed on the (001) surface of $(TMTSF)_2PF_6$. The model bilayers consist of a monolayer of naphthalene molecules adsorbed on a cation layer of $(TMTSF)_2PF_6$. The electronic band structures of an isolated cation layer and model bilayers were obtained by using the EHTB electronic band structure method.[32,33] In calculating the $\rho(r_0, E_f)$ plots, the tip−adsorbate distance r_0 was taken to be 0.5 Å above the highest-lying atom of the adsorbed naphthalene. The atomic orbitals used for our EHTB calculations are single-ζ type Slater orbitals.[33]

3. Results and Discussion

A. Pristine (001) Surface. At room temperature the crystal structure of $(TMTSF)_2PF_6$ is triclinic and belongs to the space group $P\bar{1}$ with unit cell parameters $a = 7.297$ Å, $b = 7.711$ Å, $c = 13.522$ Å, $\alpha = 83.39°$, $\beta = 86.27°$, $\gamma = 71.01°$, and $Z = 1$.[34] The *ab*- and *bc*-plane projection views of $(TMTSF)_2PF_6$ are shown in Figure 1a and b, respectively. The PF_6^- anions show considerable thermal motion with random orientations and reside at the inversion center of the unit cell.[34,35] The important structural feature of $(TMTSF)_2PF_6$ is the zig-zag columnar stacking of TMTSF molecules parallel to the *a* axis with the distance *a*/*2* between adjacent TMTSF molecules. The TMTSF stacks form 2D molecular layers parallel to the *ab* plane, where adjacent TMTSF molecules have short intermolecular Se···Se contacts.[35] All the STM images presented in this study were acquired on the largest (001) surface.

$(TMTSF)_2X$ have layers of donor cations $TMTSF^{0.5+}$ alternating with layers of X^- anions (cf. Figure 1), so that the (001) surface (i.e., the *ab*-plane surface) of a crystal sample can be terminated either with an anion layer or with a cation layer. The interpretation of the STM images recorded for the (001) surface of $(TMTSF)_2X$ ($X = PF_6^-$, ClO_4^-) in air is not unequivocal. The STM study by Fainchtein and Murphy[36] attributed the bright spherical spots of the observed STM images to the anions. Li et al.[37] re-examined the (001) surface of $(TMTSF)_2ClO_4$ by STM and also concluded that their STM images correspond to the anion layer. However, this conclusion is inconsistent with numerous STM studies of other organic conducting salts based on the donor molecule bis(ethylenedithio)tetrathiafulvalene (BEDT-TTF)[28−30,38−40]; these studies show that the STM images are almost exclusively recorded for the cation layer. This is due most likely to the fact that the cation layers are more stable against etching by the STM tip than are

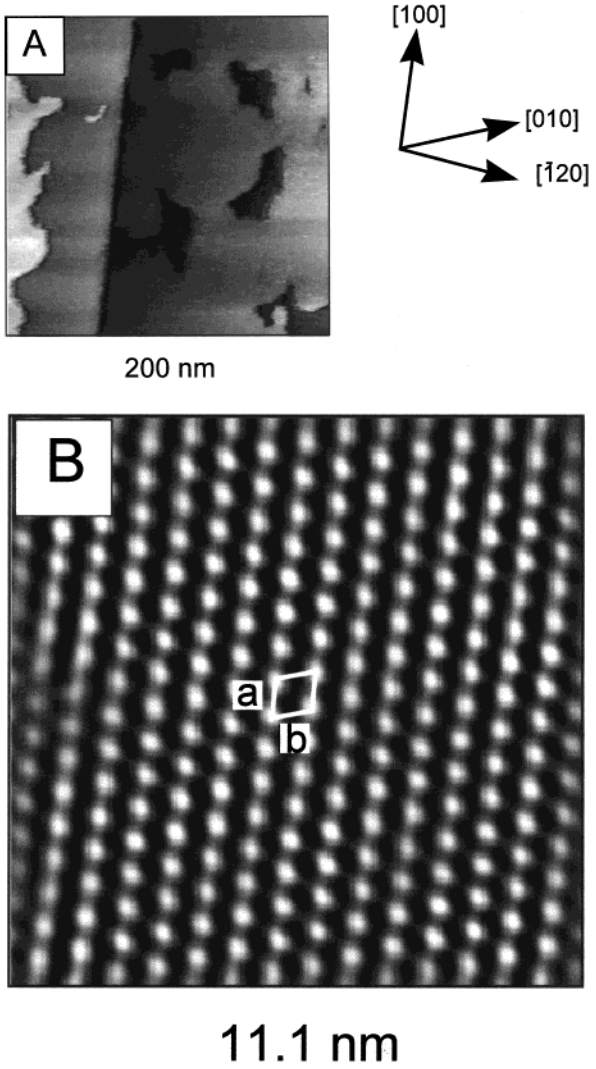

Figure 2. STM height images obtained for the (001) surface of $(TMTSF)_2PF_6$ in air: (a) nanometer-scale image and (b) filtered molecular-scale image. Tunneling conditions: the bias voltage $V_{bias} = -200$ mV and the set-point current $I_{set-point} = 1$ nA. The image in (b) was 2D Fourier filtered.

the anion layers made up of discrete anions. Thus, even when an anion layer constitutes the topmost surface layer of a crystal sample, it is etched away by the scanning tip so that the underlying cation layer is eventually imaged.[28,30] When an anion layer is composed of polymeric chains as in the case of κ-$(BEDT\text{-}TTF)_2Cu(NCS)_2$,[15] its stability against etching is enhanced, hence making it possible to detect the anion layer by STM and AFM. This observation suggests that the STM image recorded for the (001) surface of $(TMTSF)_2X$ should correspond to the cation layer rather than the anion layer.

Figure 2a presents a nanometer-scale STM image recorded for the (001) surface of $(TMTSF)_2PF_6$. The image shows adjacent terrace regions separated by steps of $\sim 14.0 \pm 0.7$ Å, which is close to the *c* lattice parameter. The step edges are all oriented in the [100] direction, i.e., the stacking direction of the TMTSF molecules. Zooming into the terrace regions produces molecular-resolution images presented in Figure 2b, which shows a repeat pattern of bright circular spots. This image is essentially identical in nature with those reported by Fainchtein and Murphy[36] and by Li et al.[37] The lattice parameters deduced from the image of Figure 2b are on average $a = 7.06 \pm 0.35$ Å, $b = 7.93 \pm 0.39$ Å, and $\gamma = 70.7 \pm 0.4°$. These parameters agree well with the corresponding values determined

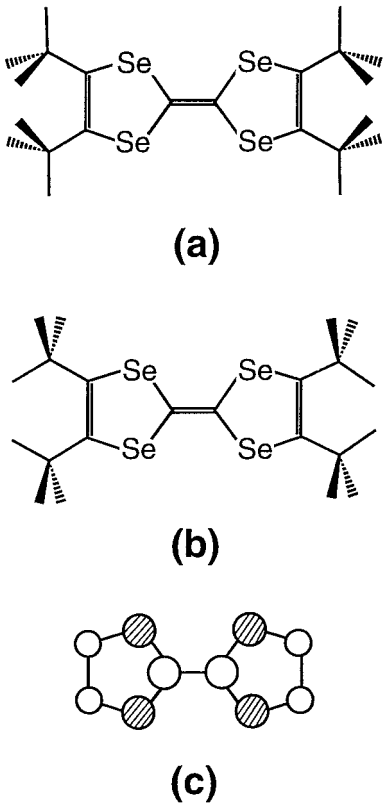

Figure 3. (a, b) Two extreme conformations of the methyl groups of TMTSF employed for the partial density plot calculations. (c) Projection view of the HOMO of TMTSF.

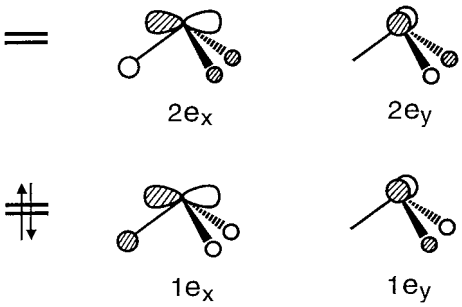

Figure 4. π-Type group orbitals of a methyl group that can interact with the HOMO of TMTSF. Here the molecular plane of TMTSF is assumed to be the *yz*-plane.

by X-ray crystallography.[34] Identical images were obtained in air as well as in solution under potential control and independently of the polarity of the bias voltage. These observations are indicative of the fact that the (001) surface images of $(TMTSF)_2PF_6$ obtained in air and in solution are unreconstructed. The independence of the image on the polarity of the bias voltage indicates the metallic character of the examined surface.

To calculate the partial density plot $\rho(r_0, E_f)$ for the cation layer of $(TMTSF)_2PF_6$, the methyl group conformations of TMTSF should be fixed. The two extreme conformations of the methyl groups are depicted in Figure 3a and b, where one hydrogen of each methyl group lies in the molecular plane of TMTSF. The nodal properties of the highest occupied molecular orbital (HOMO) of TMTSF, which is a π-type orbital, are shown in Figure 3c. The π-type group orbitals of a methyl group[41] that can interact with the HOMO of TMTSF are shown in Figure 4, where the molecular plane of TMTSF is assumed to be the *yz*-plane. For the methyl group conformations of Figure 3a and b, the $1e_x$ and $2e_x$ orbitals of each methyl group can mix

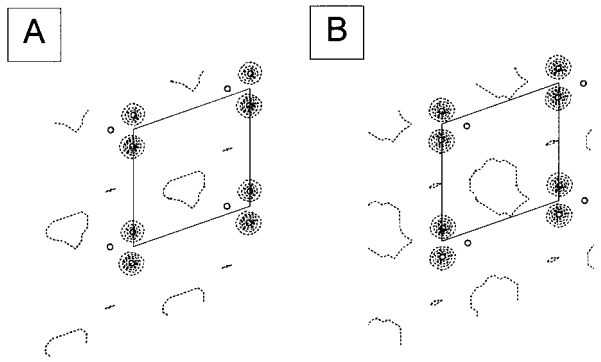

Figure 5. $\rho(r_0, E_f)$ plots calculated for the cation layer of $(TMTSF)_2PF_6$. The methyl groups of the TMTSF molecules were assumed to have the conformation of Figure 3a in the density plot (a), and the conformation of Figure 3b in the density plot (b). The plot area consists of four unit cells, and the oblique unit cell has been indicated. The contour lines correspond to 0.15, 0.30, 0.46, 0.60, and 0.76×10^{-5} electrons/au^3. The H atoms of the most protruding methyl group of TMTSF are represented by small circles.

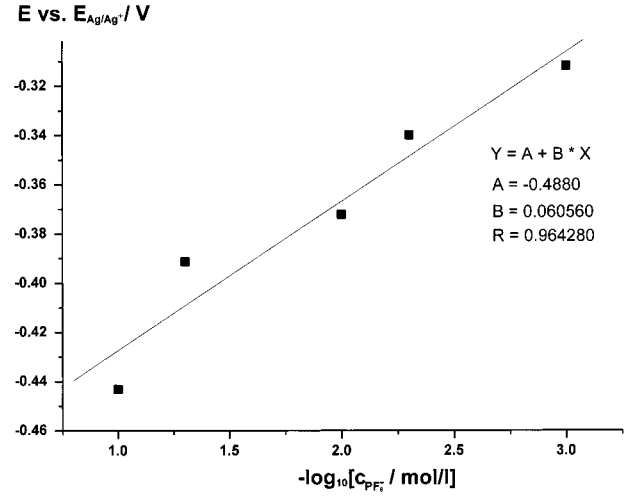

Figure 6. Variation in cell potential versus $-\log c_{PF_6^-}$ for a $(TMTSF)_2PF_6$ single-crystal electrode. The solid line represents a least-squares fit to the experimental data.

with the HOMO of TMTSF, but the $1e_y$ and $2e_y$ orbitals cannot. Thus, for each methyl group of Figure 3a and b, only the two out-of-plane hydrogen atoms contribute their orbital character to the HOMO of TMTSF, and hence to the energy levels around the Fermi level of $(TMTSF)_2PF_6$ that are mainly constructed from the HOMOs of TMTSF molecules. Figure 5a and b show the $\rho(r_0, E_f)$ plots calculated for a single cation layer in which the TMTSF molecules possess the methyl group conformations shown in Figure 3a and b, respectively. The small circles of Figure 5a and b represent the three hydrogen atoms of the most protruding methyl group of TMTSF on the (001) surface. In both partial density plots only the out-of-plane hydrogen atoms of the most protruding methyl group contribute to the partial electron density, as expected. The methyl groups of TMTSF can rotate freely around the C−C bonds. For any methyl group conformation in which none of the three hydrogen atoms lies in the molecular plane of TMTSF, all of the π-type group orbitals can interact with the HOMO of TMTSF. Thus in the STM image of the (001) surface, each TMTSF will be represented by the three hydrogen atoms of the most protruding methyl group, and these hydrogen atoms as a whole will appear as a single circular bright spot. This explains why each TMTSF appears as a bright circular spot in the STM images recorded for the cation layer of $(TMTSF)_2PF_6$. This result is consistent with the observation from the STM studies of organic conducting salts based on BEDT-TTF that the cation layer STM images are dominated by the ethylene group hydrogen atoms on the surface.[28−30]

It should be noted that the anions residing in the pockets formed by the TMTSF molecules on the (001) surface are quite mobile. Potentiometric measurements conducted on single-crystal electrodes of $(TMTSF)_2PF_6$ in our group demonstrated that these act like sensitive PF_6^--selective solid-state electrodes, thereby indicating a high mobility of the PF_6^- anions. A dynamic equilibrium should exist between the anions in solution and on/in the crystal, leading to an interfacial potential so that the anion surface coverage is determined by the electrochemical potential of the anion and depends on the interfacial potential and the concentration of the anions in solution. Thus, the variation of the cell potential as a function of $-\log c_{PF_6^-}$ results in a Nernstian response as shown in Figure 6, where the plot of the cell potential versus $-\log c_{PF_6^-}$ is linear with a slope of 60.5 mV. The latter is close to the theoretically expected value of 59.5 mV. Thus, even if the PF_6^- anions were to form the surface layer, it is highly probable that they are removed by the tip, thus exposing the cation-terminated surface at least within the region imaged by STM.

Furthermore, on an anion-covered surface area, electroneutrality would force the anions etched out by the tip to stay around the tip and cover the cation surface back as soon as the tip moves away from the etched area.

B. Naphthalene-Adsorbed (001) Surface of $(TMTSF)_2PF_6$. Naphthalene molecules spontaneously condensed into a close-packed 2D monolayer film in a long-range ordered, single-domain structure on the (001) surface of $(TMTSF)_2PF_6$ when the substrate was brought into contact with a saturated solution of naphthalene dissolved in propylene carbonate or phenyloctane either under potential control in an electrochemical environment or at open circuit potential. Identical and reproducible naphthalene overlayer structures were produced by exposure of a freshly mounted $(TMTSF)_2PF_6$ crystal to naphthalene vapor for time periods of 2−3 min. Figure 7a displays a large area scan of the naphthalene-adsorbed (001) surface of $(TMTSF)_2PF_6$. There is no evidence for any gross morphological change induced by naphthalene deposition, e.g., three-dimensional nucleation and growth. The large-scale structure of adjacent terraces and single-molecule-height steps observed for the pristine (001) surface of $(TMTSF)_2PF_6$ remains intact. Figure 7b and c shows molecular-resolution STM images revealing an elongated bright spot in each repeat unit, which we assign to individual naphthalene molecules (see below for details). The repeat distances estimated from the images are $a = 7.68 \pm 0.38$ Å and $b = 7.97 \pm 0.40$ Å, and the angle between the two repeat vectors is $\gamma = 69.23 \pm 0.35°$.

To determine the orientation and/or registry between the naphthalene adsorbate layer and $(TMTSF)_2PF_6$ substrate, nucleation and growth experiments were performed by imaging the (001) surface of $(TMTSF)_2PF_6$ in the supporting solution and then adding a drop of saturated naphthalene solution into the cell. The STM tip was engaged shortly after the naphthalene solution was introduced. This approach was necessary because attempts to selectively remove the naphthalene overlayer by reducing the tunneling gap resistance to expose the underlying substrate were unsuccessful. A high-resolution image of an "incomplete" naphthalene monolayer in the process of film formation is presented in Figure 8 (as indicated by arrows), which reveals both the pristine and naphthalene-adsorbed (001) surface areas of $(TMTSF)_2PF_6$ (the top and bottom parts of the image, respectively). This image is the middle one in a sequence

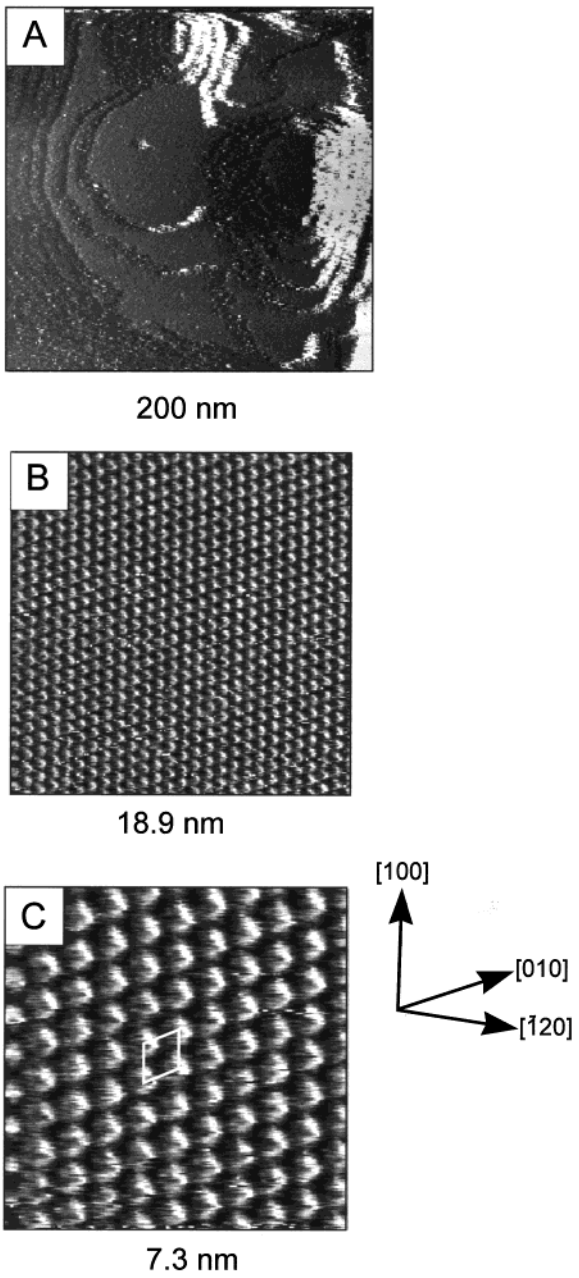

Figure 7. Unfiltered STM images of the naphthalene monolayer on the (001) surface of $(TMTSF)_2PF_6$ acquired in situ: (a) Large-scale, height-shaded image and (b, c) high-resolution images. Tunneling conditions: (a) $V_{bias} = -200$ mV, $I_{set-point} = 2$ nA. (b, c) $V_{bias} = -200$ mV, $I_{set-point} = 1.5$ nA. The primitive unit cell for the naphthalene adlayer is indicated.

of three successive images which show the monolayer growing across the crystal surface from the top to the bottom. The image is a true reflection of the dynamics of naphthalene monolayer formation and is not a result of a destructive removal of physisorbed organic monolayers by the STM tip or a result of a sudden change in tip condition. This is supported by the fact that the image was scanned from the top to the bottom and because on close inspection, the edge of the monolayer is not perfectly straight or aligned precisely along the scan direction. The image of Figure 8 allows us to determine the orientation of the naphthalene adsorbate layer with respect to the underlying substrate unambiguously. The overlayer lattice is unrotated with respect to the substrate lattice, and the repeat vectors of the overlayer lattice are aligned along the [100] and [010] directions of the substrate lattice. Within experimental error these observations are consistent with a commensurate pseudomorphic (1×1) naphthalene overlayer structure.

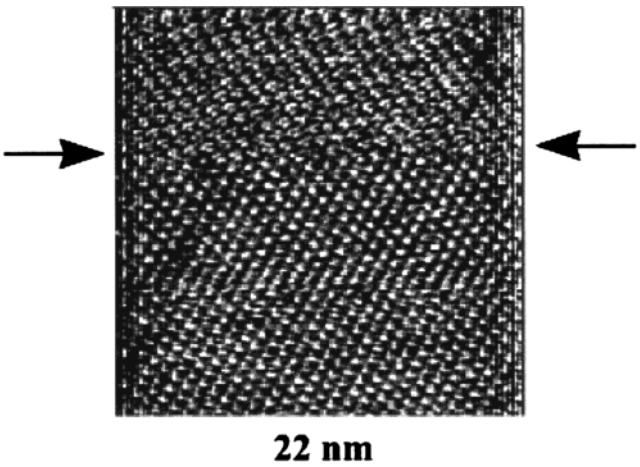

Figure 8. Unfiltered high-resolution STM image of the nucleation and growth of the naphthalene monolayer phase on the (001) surface of $(TMTSF)_2PF_6$ acquired in situ. Tunneling conditions: $V_{bias} = -200$ mV; $I_{set-point} = 1$ nA. The image was scanned in the direction from top to bottom. Arrows highlight the position of the naphthalene overlayer structure.

We have not observed any experimental evidence for bulk naphthalene growth following the formation of the naphthalene monolayer phase. The growth of this layer is therefore self-limiting. In addition, there are no layered motifs in the bulk naphthalene structure[42] (monoclinic prismatic, space group $P21/a$) which are compatible with the observed naphthalene monolayer structure as determined by STM.

The STM image contrast does not vary with changing tunneling parameters. High-quality images of the naphthalene-covered surface were produced at sample biases of either polarity. Identical images were obtained for different tips, and there was no evidence for a reconstruction of the STM tip. Furthermore, the same tip was employed for all STM images presented in this study.

The naphthalene overlayers are surprisingly stable toward repeated scanning in either scan direction and at low tunneling gap resistances (involving high set-point currents and small tunneling biases). Furthermore, we could image the same naphthalene adlayer structure with molecular resolution even after the samples were exposed to the ambient laboratory air over several days.

In high-resolution STM images of naphthalene adlayers on surfaces of transition metals,[22−26] each naphthalene appears most commonly as a double-lobed structure of uniform intensity. This is expected from its two-ring structure if the molecule lies flat on the surface. In the present case the bright elongated spot representing each naphthalene molecule shows a distinct modulation in image contrast. In accordance with the discussion of the previous section, the STM images observed in our study refer most probably to the naphthalene molecules adsorbed onto the cation-terminated surface of $(TMTSF)_2PF_6$. The naphthalene can favorably interact via its π-electron clouds with the methyl group hydrogen atoms of TMTSF on the (001) surface. One might consider the naphthalene overlayer on the (001) surface of $(TMTSF)_2PF_6$ as a physisorbed overlayer in which the "lateral interaction" between naphthalene molecules is stronger than the "vertical interaction" between naphthalene and TMTSF. However the formation of a commensurate pseudomorphic (1×1) naphthalene structure indicates that the (001) surface of $(TMTSF)_2PF_6$ acts as a template for the adsorption of naph-

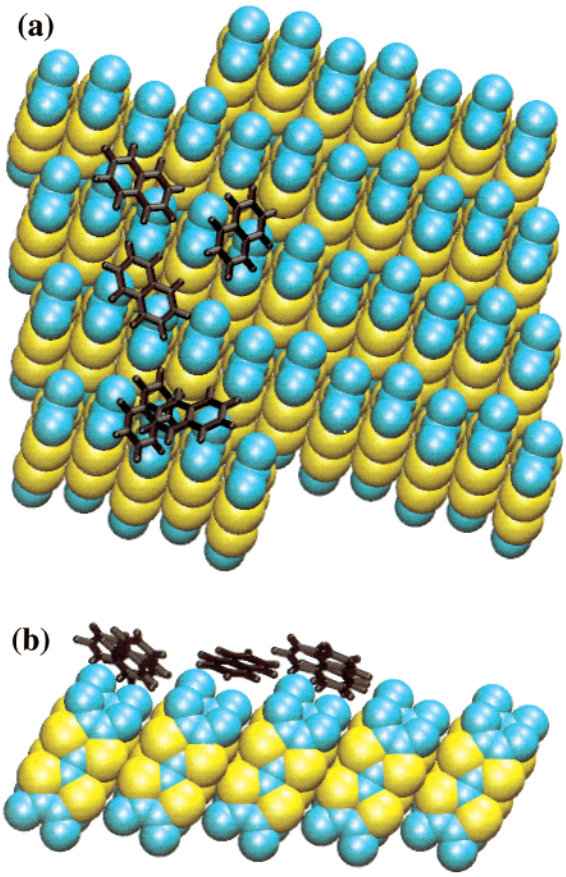

Figure 9. Orientation of a single naphthalene molecule at the end of each of the five successive simulated Monte Carlo annealing calculations overlaid and presented in (a) normal view and (b) side view as determined on the constructed (001) plane slab of the cation-terminated surface. It should be emphasized that there are no naphthalene−naphthalene intermolecular interactions present.

thalene. An identical monolayer structure of naphthalene was generated by various deposition methods. On the basis of the STM data alone it is impossible to work out the exact adsorption geometry of the naphthalene and determine its preferential adsorption sites on the (001) surface of $(TMTSF)_2PF_6$.

C. Monte Carlo Simulation. To determine the adsorption geometry and the potential binding sites for the naphthalene on the (001) surface of $(TMTSF)_2PF_6$, we performed Monte Carlo simulations. The interaction of a single naphthalene molecule with a cluster of TMTSF molecules representing the (001) surface cation layer was modeled by van der Waals forces. The simulation did not include naphthalene−naphthalene interactions. The result of the simulation is presented in Figure 9, which shows the five successive positions adopted by a single naphthalene molecule during the five simulated annealing steps in the calculation (cf. Experimental Section). Table 1 lists the tilt angles of the naphthalene molecule extracted from the simulation study. A single naphthalene molecule is rotationally disordered upon adsorption onto the cation surface. Nevertheless, the preferred adsorption sites for isolated naphthalene molecules are definitely located within the "molecular grooves" created by the zig-zag columnar stacking of the respective TMTSF molecules on the (001) surface.

D. Partial Electron Density Plot Calculations. To consider probable arrangements of naphthalene molecules on the cation-terminated (001) surface of $(TMTSF)_2PF_6$, we need to examine the surface corrugation. A schematic projection view of $(TMTSF)_2PF_6$ along the *a* axis direction is shown in Figure 1b.

TABLE 1: Molecular Tilt Angles for a Single Naphthalene Molecule with Respect to Cation-Terminated (001) Surface of $(TMTSF)_2PF_6$ for Its Long and Short C_2 Molecular Axis as Derived from the Five Successive Monte Carlo Simulated Annealing Procedure Results Presented in Figure 9

naphthalene tilt angles wrt. short molecular C_2 axis	naphthalene tilt angles wrt. long molecular C_2 axis
24.23°	27.34°
20.25°	23.03°
18.29°	8.99°
23.59°	29.0°
37.59°	18.07°

The surface of the layer is made up of the methyl group hydrogen atoms of the TMTSF molecules. Each TMTSF molecule is inclined to the (001) surface by the angle $\theta = 32°$. In each stack of TMTSF molecules, the heights of the molecules with respect to the surface show an alternation. Thus each plane defined by four methyl groups of two adjacent TMTSF molecules within a TMTSF stack is inclined to the (001) surface by the angle $\phi = 20°$. For convenience, the surface area defined by four such methyl groups will be referred to as a "four-methyl-step". The plane of each four-methyl-step is tilted from the (001) by the angles $\theta = 32°$ and $\phi = 20°$. As measured by the positions of the hydrogen atoms, each four-methyl-step has a rectangular shape with dimensions $\sim 5 \times \sim 6$ Å (longer along the intrastack direction), and a naphthalene molecule can be contained in a rectangle of dimensions $\sim 5 \times \sim 7$ Å. For a naphthalene molecule to be adsorbed flat on the cation-terminated surface, each four-methyl-step will be an ideal place. In such an adsorption, the methyl group C−H bonds of TMTSF will be in contact with the π electron clouds of naphthalene. Such contacts are frequently found in molecular crystals of flat compounds and provide van der Waals interactions. Thus, the four-methyl-steps are ideal adsorption sites for naphthalene molecules. Each naphthalene adsorbed flat on a four-methyl-step has its molecular plane tilted from the (001) surface by the angles $\theta = 32°$ and $\phi = 20°$. Thus, given the carbon-atom numbering for naphthalene in Figure 10a, the three carbon atoms at one corner of naphthalene become the highest-lying carbon atoms (e.g., C1, C2, and C3).

To help interpret the observed STM images, we calculate the partial electron density plots $\rho(r_0, E_f)$ for model bilayers,[28−31] which consist of a naphthalene monolayer and a cation layer lying below. As discussed above, we consider that each four-methyl-step of a cation layer is an adsorption site for naphthalene. There are many possible parallel arrangements between a naphthalene molecule and a four-methyl-step. Our consideration will be limited to the case when the plane of a naphthalene molecule lies 3.0 Å above that of the highest-lying hydrogen atoms of a four-methyl-step (the H···C van der Waals distance is about 2.9 Å). In addition, we consider only the extreme arrangements in which the center of a naphthalene molecule lies above that of a four-methyl-step. In these arrangements, the long axis of naphthalene can be either parallel or perpendicular to the longer side of a four-methyl-step (Figure 10b and c, respectively). Hereafter, these orientations of an adsorbed naphthalene molecule will be referred to as the 0° and 90° orientations, respectively. To simulate the (1×1) superstructure STM images, we construct the corresponding model bilayers of composition $(TMTSF)_4^{2+}$(naphthalene).

The nodal properties of the HOMO and lowest unoccupied molecular orbital (LUMO) of naphthalene are schematically presented in Figure 11a and b. The atomic coefficient of the C1, C4, C5, and C8 atoms is larger than that of the C2, C3, C6, and C7 atoms. The π-orbitals of adsorbed naphthalene

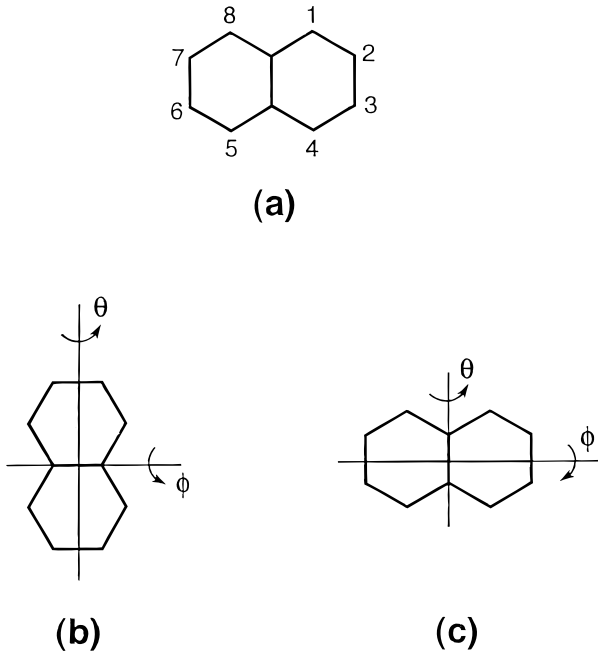

Figure 10. (a) Atom numbering for naphthalene. Two extreme orientations of naphthalene adsorbed on a four-methyl-step of the (001) cation layer surface of $(TMTSF)_2PF_6$: (b) 0° orientation and (c) 90° orientation.

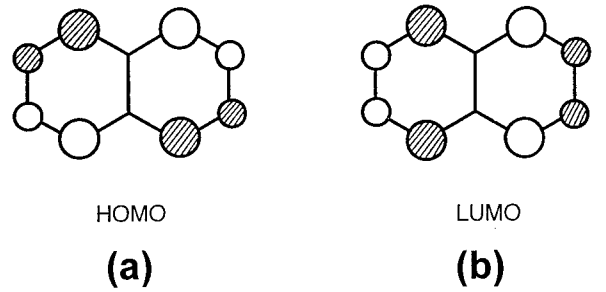

Figure 11. Nodal properties of the (a) HOMO and (b) LUMO of naphthalene.

molecules mix weakly into the energy levels of the conduction bands of the underlying cation layer. Because only the STM images acquired at negative sample biases are presented in this work, we calculate the partial density plots of a model bilayer system using the occupied energy levels lying between E_f and $E_f - \Delta$, where E_f is the Fermi level of the cation layer, and the energy window Δ is 0.25 eV.[28−31] Our EHTB calculations show that the conduction bands of an isolated cation layer, which are largely constructed from the HOMOs of TMTSF molecules, has the width of 0.60 eV. Our EHTB calculations show that the HOMO of naphthalene lies about 3.75 eV below E_f, and the LUMO of naphthalene about 0.7 eV below E_f. In a one-electron picture, it would imply an oxidation of TMTSF by naphthalene. This erroneous implication is a consequence of the fact that the EHTB method does not adjust the effective Hamiltonian self-consistently. However, this problem does not affect our analysis as long as partial density plots are calculated using the energy window between E_f and $E_f - \Delta$ of the cation layer.

Figure 12a shows the $\rho(r_0, E_f)$ plot calculated for the (1×1) model bilayer in which each naphthalene molecule has the 0° orientation. The corresponding plot for the 90° orientation is shown in Figure 12b. The three circles in each unit cell of these plots refer to the three highest-lying carbon atoms of naphthalene (i.e., C1, C2, and C3). In essential shape, the two $\rho(r_0, E_f)$ plots

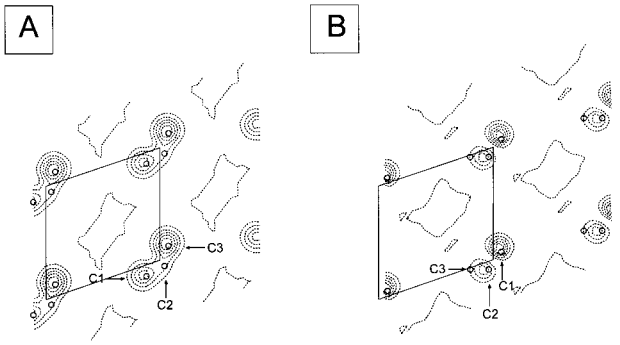

Figure 12. Partial density plots $\rho(r_0, E_f)$ of the $(TMTSF)_4^{2+}$-(naphthalene) calculated for the (1×1) model bilayer in which each naphthalene molecule has the (a) 0° and (b) 90° orientations. The plot area consists of four neighboring unit cells. The contour values used are 0.13, 0.26, 0.39, 0.51, 0.64, and 0.99×10^{-9} electrons/au^3 in (a), and 0.08, 0.17, 0.25, 0.33, 0.41, and 0.50×10^{-9} electrons/au^3 in (b).

are similar. In detail, they are slightly different; the plot is mainly represented by the densities of the C1 and C3 atoms in the 0° orientation (Figure 12a), and by the C1 and C2 atoms in the 90° orientation (Figure 12b). This small difference between the 0° and 90° orientations reflects the fact that the registry between the four-methyl-step and naphthalene molecule is different for the two orientations, and so is the extent of overlap between the orbitals of the adsorbate and substrate. The calculated partial electron density plots are in excellent agreement with the STM images (Figure 7b and c) and clearly reproduce the contrast modulation observed in the elongated bright pattern representing each naphthalene molecule. This result therefore confirms that the naphthalene molecules assume a tilted configuration upon adsorption onto the four-methyl-steps of the cation-terminated (001) surface of $(TMTSF)_2PF_6$. However, it is virtually impossible to distinguish between the 0° and 90° orientations of the naphthalene on the basis of the experimental STM data, so we have to assume that both arrangements are feasible options.

4. Concluding Remarks

Our high-resolution STM images recorded for the pristine (001) surface of $(TMTSF)_2PF_6$ show a 2D repeat pattern of circular bright spots. These images are essentially the same as those recorded for the (001) surface of $(TMTSF)_2X$ ($X = PF_6^-$, ClO_4^-) by Fainchtein and Murphy[36] and by Li et al.[37] Our analysis indicates that these STM images correspond to the cation layers of these salts, and that each circular bright spot represents the three hydrogen atoms of the most protruding methyl group of each TMTSF molecule on the (001) surface.

Our study of naphthalene-adsorbed (001) surface of $(TMTSF)_2PF_6$ indicates that the preferential adsorption sites for naphthalene are the "steps" defined by the four methyl groups of two adjacent TMTSF molecules within each TMTSF stack. The plane of each four-methyl-step is tilted from the (001) surface by the angles $\theta = 32°$ and $\phi = 20°$, and one naphthalene molecule can lie flat on each four-methyl-step. This structural model explains the mechanical stability of the naphthalene monolayer films toward tip−sample forces during extended scanning. In contrast to "atomically smooth" surfaces, the (001) surface of $(TMTSF)_2PF_6$ is corrugated such that naphthalene molecules can lodge themselves on the "four-methyl-steps" of the molecular grooves and become virtually immobilized on this surface.

A combination of STM measurements, partial electron density plot calculations, and Monte Carlo simulations provides a systematic route to analyze and determine the mechanisms

governing molecular self-assembly processes on organic conducting crystal surfaces. It is hoped that the insight gained from the present study will help guide future studies on the heteroepitaxial nucleation and growth of more complicated molecular architectures with exciting new properties.

Acknowledgment. The work at North Carolina State University was supported by the Office of Basic Energy Sciences, Division of Materials Sciences, U. S. Department of Energy, under Grant DE-FG05-86ER45259. J. W. Essex acknowledges receipt of a Royal Society Fellowship by the Royal Society. The work at the University of Southampton was supported by the Leverhulme Trust. N. Robertson acknowledges receipt of a BP/Royal Society of Edinburgh Fellowship. I. S. Nandhakumar wishes to thank K. Bechgaard for helpful discussions.

References and Notes

(1) Baizer, M. M. *Organic Electrochemistry*; Plenum Press: New York, 1991.

(2) Murray, R. W. In *Molecular Design of Electrode Surfaces*; Murray, R. W., Ed.; J. Wiley: New York, 1992; p 1.

(3) Lehn, J. M. *Angew. Chem., Int. Ed. Engl*. **1988**, *27*, 89.

(4) Carter, F. L., Ed. *Molecular Electronic Devices*; Marcel Dekker: New York, 1982.

(5) Nichols, R. J.; Beckmann, W.; Meyer, H.; Batina, N.; Kolb, D. M. *J. Electroanal. Chem*. **1992**, *330*, 381.

(6) Nichols, R. J.; Bach, C. E.; Meyer, H. *Ber. Bunsen-Ges. Phys. Chem*. **1993**, *97*, 1012.

(7) Service, R. F. *Science* **1997**, *278*, 383.

(8) Chiang, S. In *Scanning Tunneling Microscopy I*; Wiesendanger, R., Güntherodt, H.-J., Eds.; Springer-Verlag: Berlin, 1991; pp 181−205.

(9) Tao, N. J.; De Rose, J. A.; Lindsay, S. M. *J. Phys. Chem*. **1993**, *97*, 910.

(10) Cunha, F.; Tao, N. J. *Phys. Rev. Lett*. **1995**, *75*, 2376.

(11) Tao, N. J.; Shi, Z.*J. Phys. Chem*. **1994**, *98*, 1464.

(12) (a) Ribault, M.; Moradpour, A. *J. Am. Chem. Soc*. **1998**, *120*, 7993. (b) Last, J. A.; Hooks, D. E.; Hillier, A. C.; Ward, M. D. *J. Phys. Chem. B* **1999**, *103*, 6723. (c) Hooks, D. E.; Yip, C. M.; Ward, M. D. *J. Phys. Chem. B* **1998**, *102*, 9958. (d)Last, J. A.; Hillier, A. C.; Hooks, D. E.; Maxson, J. B.; Ward, M. D. *Chem. Mater*. **1998**, *10*, 422.

(13) (a) Forrest, S. R. *Chem. Rev.* **1997**, *97*, 1793. (b) England, C. D.; Collins, G. E.; Schuerlein, T. J.; Armstrong, N. R. *ACS Symp. Ser*. **1994**, *561*, 202.

(14) Sleator, T.; Tysko, R. *Phys. Rev. Lett.* **1988**, *60*, 1418.

(15) Magonov, S. N.; Bar, G.; Keller, E.; Yagubskij, E. B.; Laukhina, E. B.; Cantow, H.-J. *Ultramicroscopy* **1992**, *42*−*44*, 1009.

(16) Fainchtein, R.; D'Arcangelis, S. T.; Yiang, S. S.; Cowan, D. O. *Science* **1992**, *256*, 1012.

(17) Dvorak, M. A.; Ward, M. D. *Chem. Mater*. **1994**, *6*, 1386.

(18) Carter, P. W.; Hillier, A. C.; Ward, M. D. *J. Am. Chem. Soc*. **1994**, *116*, 944.

(19) Bartlett, P. N.; Tong, X. Q. *J. Phys. Chem*. **1997**, *101*, 8540.

(20) Gland, J. L.; Somorjai, G. A. *Surf. Sci.* **1973**, *38*, 157.

(21) Bardi, U.; Magnanelli, S.; Rovida, G. *Langmuir* **1987**, *3*, 159.

(22) Yau, S.-L.; Kim, Y.-G.; Itaya, K. *J. Phys. Chem*. **1997**, *101*, 3547.

(23) Yau, S.-L.; Itaya, K. *Colloids Surf*. **1998**, *134*, 21.

(24) Wan, L.-J.; Itaya, K. *Langmiur* **1997**, *13*, 7173.

(25) Hallmark, V. M.; Chiang, S.; Brown, J. K.; Wöll, Ch. *Phys. Rev. Lett*. **1991**, *66*, 48.

(26) Hallmark, V. M.; Chiang, S.; Wöll, Ch. *J. Vac. Sci. Technol*. **1991**, *9*, 1111.

(27) Bechgaard, K.; Jacobsen, C. S.; Mortensen, K.; Pedersen, H. J.; Thorup, N. *Solid State Commun*. **1980**, *33*, 1119.

(28) Magonov, S. N.; Whangbo, M.-H. *Surface Analysis with STM and AFM*; VCH: Weinheim, 1996.

(29) Magonov, S. N.; Whangbo, M.-H. *Adv. Mater*. **1994**, *6*, 355.

(30) Bar, G.; Magonov, S. N.; Cantow, H.-J.; Kushch, N. D.; Yagubskii, E. B.; Liang, W.; Ren, J.; Whangbo, M.-H. *New J. Chem*. **1993**, *17*, 439.

(31) Seo, D.-K.; Ren, J.; Whangbo, M.-H. *Surf. Sci*. **1997**, *370*, 252.

(32) Whangbo, M.-H.; Hoffmann, R. *J. Am. Chem. Soc*. **1978**, *100*, 6093.

(33) Our calculations were carried out by employing the *CAESAR* program package (Ren, J., Liang, W., Whangbo, M.-H. *Crystal and Electronic Structure Analysis Using CAESAR*, 1998. This book can be downloaded free of charge from the website http://www. PrimeC.com/.).

(34) Thorup, N.; Rindorf, G.; Soling, H.; Bechgaard, K. *Acta Crystallogr*. **1981**, *37*, 1236.

(35) Ferraro, J. R.; Williams, J. M., Eds. *Introduction to Synthetic Electrical Conductors*; Academic Press: Orlando, FL, 1987.

(36) Fainchtein, R.; Murphy, J. C. *J. Vac. Sci. Technol*. **1991**, *9*, 1013.

(37) Li, S.; White, H. S.; Ward, M. D. *J. Phys. Chem. B* **1992**, *96*, 9014.

(38) Bando, H.; Kashiwayo, S.; Tokumoto, H.; Anzai, H.; Kinoshita, N.; Kajimura, K. *J. Vac. Sci. Technol*. **1990**, *8*, 479.

(39) Magonov, S. N.; Bar, G.; Keller; Yagubskij, E. B.; Cantow, H.-J. *Synth. Met*. **1991**, *40*, 247.

(40) Yoshimura, M.; Shikegawa, H.; Nejoh, H.; Saito, G.; Saito, Y.; Kawazu, A. *Phys. Rev. B* **1991**, *43*, 13590.

(41) Albright, T. A.; Burdett, J. K.; Whangbo, M.-H., *Orbital Interactions in Chemistry*; Wiley: New York, 1985; Ch. 9.

(42) Abrahams, S. C.; Monteath Robertson, J. *Acta Crystallogr*. **1949**, *2*, 233.